AERODYNAMIC DESIGN OF SWEPT INFINITE WING WITH FLAP FOR SUBSONIC AND TRANSONIC FLIGHT REGIMES

K. V. Kovalev

Moscow Institute of Physics and Technology
Zhukovsky, Russia

Abstract

The methodology is based on the solution of the full potential equation in conservative form with the combined boundary conditions, in which the no flux condition is set on one part of the wing surface, and the specified pressure distribution is set on another part.The solution of this problem results in the surface distribution of the normal velocity determining. Then the wing shape is changed according to this distribution. This process may be repeated until convergence.
The trailing edge closure is provided by means of specifying of the additional normal velocity distribution on the surface. Such an approach allows to control various shape parameters, thickness or camber distribution, etc.
Full potential equation is solved using the finite-difference method in the curvilinear airfoil and flap surfaces-fitted coordinate system. The spatial potential derivatives are approximated by central-difference scheme in subsonic regions of the flow and by upwind-difference scheme in supersonic those, both schemes are of the second order of accuracy. The system of finite-difference equations is solved by Newton's procedure, the linear system being solved by the incomplete LU factorization method and with acceleration by GMRES(k).
The results include different test design cases, demonstrating the abilities of the current design method.

Introduction

Nowadays creation of up-to-date transonic aerodynamic configurations requires applying accurate enough and reliable numerical methods for their design. First of all one may mention optimization methods, full inverse and mixed inverse methods.
Optimization methods couple conventional analysis method with an optimization algorithm to modify iteratively the geometry in order to minimize some special function (for example, a drag) and are the most perspective design methods. Unfortunately, a successful use of these methods depend a lot upon an accuracy of the flow analysis method applied, and it is most preferable to use for this purpose the Reynolds-averaged Navier-Stokes equations, which most perfectly take into account the physical features of the flow. Procedure like this is unavoidably very time-consuming, that's why optimization methods are mostly effective at a final design step. The full inverse method allows us to find the geometry, corresponding to the special velocity distribution, determined at the entire surface. But this method may be applied in general only for subsonic regimes, and it does not permits to take into account geometrical restrictions. Mixed inverse method allows design in a wide range of regimes including transonic those, and permits to take into account various geometrical restrictions, what makes this method the most preferable one for the preliminary design, but in order to use effectively of this method, designer must have enough experience and qualification when choosing a special pressure distribution. The using mixed inverse method for the preliminary design allows applying more simple flow analysis methods, such as full potential equations solution methodology or method, based on the viscous-inviscid interaction procedure.
In the present paper the mixed inverse method for the design of the infinite swept wing for subsonic and transonic flight regimes was realized. An attempt was made to use this method for the design of the infinite wing with flap for the same regimes.

Wing analysis method

Problem formulation

The calculation of a steady inviscid isentropical flow around the wing with flap is accomplished by means of the solution of the full potential equation in the conservative form. This equation looks in the Cartesian coordinate system as follows

$$(\rho\varphi_x)_x + (\rho\varphi_y)_y = 0 \qquad (1)$$

where x and y are Cartesian coordinates, φ - potential function and ρ - density, which may be determined from the expression

$$\rho = \left\{1 + \frac{\gamma - 1}{2} M_\infty^2 \left(1 - q^2\right)\right\}^{\frac{1}{\gamma - 1}} \qquad (2)$$

where M_∞ is the freestream Mach number, q - total velocity and γ - the ratio of specific heats. I n order to simplify the boundary condition, stated on the wing surface, the equation (1) is transformed to the curvilinear airfoil and flap surfaces-fitted coordinate system (fig.1).

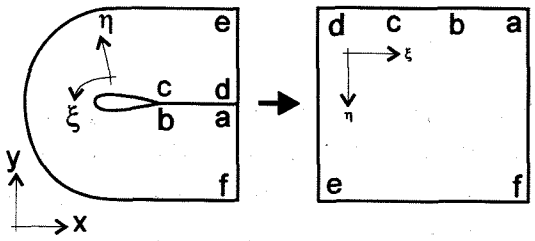

fig.1

In this coordinate system the equation has the form

$$\left(\frac{\rho U}{J}\right)_\xi + \left(\frac{\rho V}{J}\right)_\eta = 0 \qquad (3)$$

Cartesian components of the velocity are connected with its contravariant components and derivatives of potential in the curvilinear system by the expressions

$$(U\,V)^T = H^{-1}(u\,v)^T = [H^T H]^{-1}(\varphi_\xi\ \varphi_\eta)^T \qquad (4)$$

where

$$H = \begin{pmatrix} x_\xi & x_\eta \\ y_\xi & y_\eta \end{pmatrix}$$ - Jacobian, J = det H

$$[H^T H]^{-1} = \begin{pmatrix} A_1 & A_2 \\ A_2 & A_3 \end{pmatrix}$$ - metric coefficients matrix.

The no flux condition is fixed on the wing and flap surfaces. It simply means that normal to surface contravariant velocity components are equal to zero. The Cutta-Zhukovsky condition is specified on the trailing edges of the wing and flap.

The balance of the normal mass fluxes and the preserving of potential discontinuity from the trailing edge along the vortex sheet are fixed on the vortex sheet. These conditions may be expressed as follows

$$\begin{aligned} (\rho v_n)_U &= (\rho v_n)_L \\ \varphi_U - \varphi_L &= \Delta\varphi_{TE} \end{aligned} \qquad (5)$$

where $\Delta\varphi_{TE}$ - potential discontinuity on the trailing edge. Indexes "L" and "U" correspond to the lower and upper vortex sheet surfaces accordingly.
The far field condition is fixed on the outer boundary of the flow

$$\varphi_\infty = x\cos\alpha + y\sin\alpha - \frac{\Gamma}{2\pi}\theta \qquad (6)$$

where α is an attack angle

$$\theta = \operatorname{arctg}\left(\frac{\beta y}{x}\right), \quad \beta = \sqrt{1 - M_\infty^2}\,.$$

Grid generation

It is necessary to generate a grid, corresponding to the airfoil and flap surfaces-fitted curvilinear coordinate system for the solution of the full-potential equations system. A grid, generated with the help of a two-step procedure, is used in this paper.
Grid over the main element. C-type grid is generated around an airfoil without a flap by superimposing conformal transformation, used for this purpose by Jameson and Caughey [1], over the shear transformation. For this purpose airfoil contour from the physical coordinate system (fig.1) is mapped onto the upper half plane with the help of conformal transformation (7).

$$w = \sqrt{z} \qquad (7)$$

where z=x+iy, w=s+it Here the contour is represented by a curve close to Os axis. The rectangular grid generated in the transformed plane is displaced in accordance with the countour and outer boundary shape (fig.2).

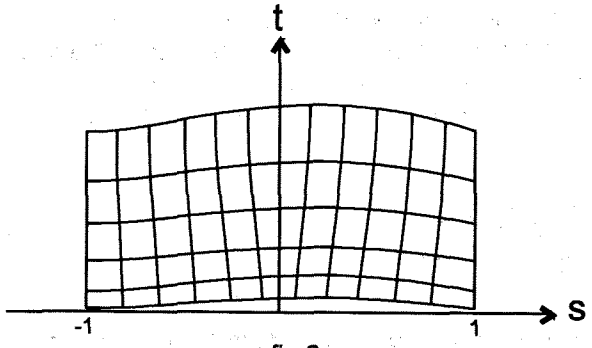

fig.2

And then, with the help of inverse transformation

$$z = w^2 \qquad (8)$$

it is mapped onto the initial xy-plane.

Modification of the grid in flap region. A rectangular domain is selected near the flap. Domain boundaries are lines j=1, j=JF2 and lines i=IF1, i=IF2, which are chosen as far from the flap as coordinate lines perturbations, induced by the flap presence, can relax enough inside this domain (fig.3).

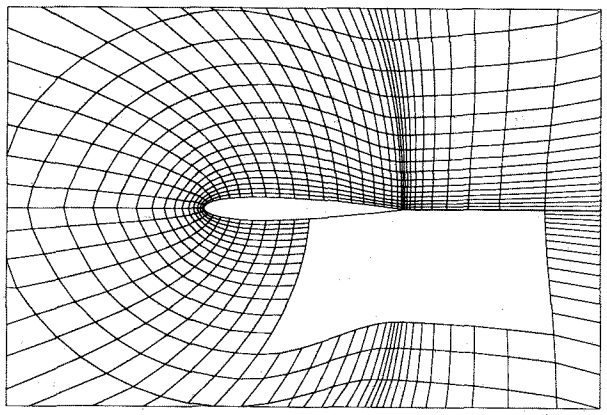
fig.3

Then coordinate lines connecting the leading and the trailing edges of a flap with vertical rectangular boundaries are constructed. Coordinate lines smoothness and grid cell sizes continuity are taken into the account. Now, in two rectangles obtained below and above the flap the grid is generated with the help of the solution of differential equations system (9)

$$\begin{cases} \xi_{xx} + \xi_{yy} = P_1(x,y) \\ \eta_{xx} + \eta_{yy} = P_2(x,y) \end{cases} \qquad (9)$$

where (x, y) - coordinates values in physical field, (ξ, η) - their values in the computantional field, where grid generation domains are rectangles. Flap surface and rectangle boundaries nodes are used as Dirichlet boundary conditions. After exchanging (x, y) and (ξ, η) equations look like

$$g_{22}\vec{r}_{\xi\xi} - 2g_{12}\vec{r}_{\xi\eta} + g_{11}\vec{r}_{\eta\eta} = Q(\xi,\eta) \qquad (10)$$

where

$$Q(\xi,\eta) = -g_{22}P_1\vec{r}_\xi - g_{11}P_2\vec{r}_\eta$$

$$g_{11} = \left|\vec{r}_\xi\right|^2,\ g_{12} = g_{21} = \vec{r}_\xi \cdot \vec{r}_\eta,\ g_{22} = \left|\vec{r}_\eta\right|^2$$

$$\vec{r} = (x\ y)^T$$

Source members P_1, P_2 are determined from the orthogonality control condition. After multiplying (10) by $\vec{r}_\xi$ and $\vec{r}_\eta$, and taking into account orthogonality condition $g_{12} = g_{21} = 0$ we can find

$$P_1 \approx -\frac{\vec{r}_{\xi\xi}\cdot\vec{r}_\xi}{g_{11}}, P_2 \approx -\frac{\vec{r}_{\eta\eta}\cdot\vec{r}_\eta}{g_{22}} \qquad (11)$$

The values of P_1, P_2 on the computational domains boundaries are calculated with the use of boundary conditions by expressions (11), and then these boundary values are interpolated inside the computational domains. System (10) is solved by the finite-difference method with the use of successive line over relaxation procedure (SLOR). The flap region of the final grid is shown on the fig.4.

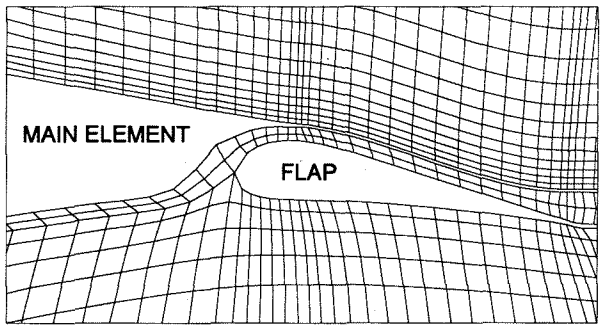

fig.4

Finite-difference approximation

The finite volume methodology is used for the numerical solution of the full potential equation. The mass fluxes through the control volume boundaries (fig.5) are expressed by the potential values in points 1-9.

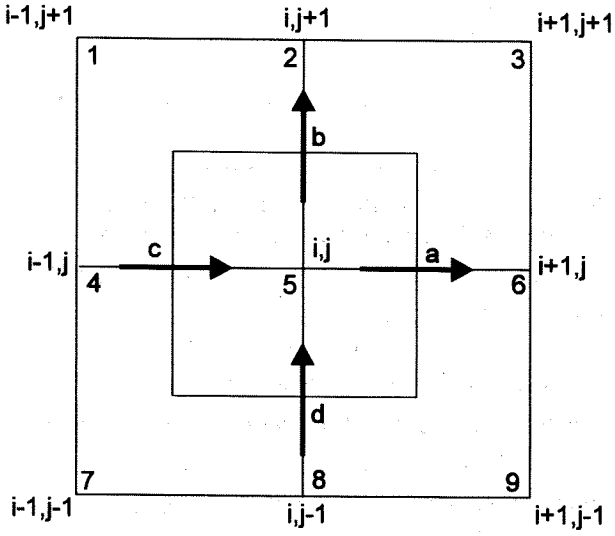

fig.5

Flux (a) may be written as follows

$$Q_{(a)} = \left(\tilde{\rho}\frac{U}{J}\right)_{i+\frac{1}{2},j} = \left(\tilde{\rho}\frac{A_1\varphi_\xi + A_2\varphi_\eta}{J}\right)_{i+\frac{1}{2},j} \qquad (12)$$

where

$$\varphi_{\xi_{i+\frac{1}{2},j}} = \varphi_{i+1,j} - \varphi_{i,j}$$

$$\varphi_{\eta_{i+\frac{1}{2},j}} = \frac{1}{4}\left(\varphi_{i+1,j+1} + \varphi_{i,j+1} - \varphi_{i+1,j-1} - \varphi_{i,j-1}\right) \qquad (13)$$

In order to provide the stability of the finite-difference scheme in supersonic domains, artificial viscosity is included into equations. For axample, according to Osher approach [2], the artificial viscosity is taken into consideration as follows

$$\tilde{\rho}_{i+\frac{1}{2},j} = \rho_{i+\frac{1}{2},j} - \frac{Q\left(q_{i+\frac{1}{2},j}\right) - Q\left(q_{i-\frac{1}{2},j}\right)}{q_{i+\frac{1}{2},j}} \qquad (14)$$

when U>0, where

$$Q(q) = \nu\left[\rho(q)q - \rho_* q_*\right], \quad \nu = \begin{cases} 1, & q \geq q_* \\ 0, & q < q_* \end{cases}$$

The scheme (14) provides first order of accuracy in supersonic regions of the flow. In the current paper the approach, described by Karas [3], is used, which provides second order of accuracy in supersonic regions. In this case the expression for density looks like

$$\tilde{\rho}_{i+\frac{1}{2},j} = \rho_{i+\frac{1}{2},j} - \frac{Q\left(q_{i+\frac{1}{2},j}\right) - Q\left(q^-_{i+\frac{1}{2},j}\right)}{q_{i+\frac{1}{2},j}} \qquad (14a)$$

where $q^-_{i+\frac{1}{2},j} = 2q_{i-\frac{1}{2},j} - q_{i-\frac{3}{2},j}$, at U>0. Finally finite-difference equation looks like

$$\tilde{\partial}_\xi\left(\tilde{\rho}\frac{U}{J}\right)_{i+\frac{1}{2},j} + \tilde{\partial}_\eta\left(\rho\frac{V}{J}\right)_{i,j+\frac{1}{2}} = 0 \qquad (15)$$

No flux condition on the surface is approximated with the use of the control volume, adjacent to the surface (fig.6), and the corresponding finite-difference equation is

$$\frac{1}{2}\tilde{\partial}_\xi\left(\tilde{\rho}\frac{U}{J}\right)_{i+\frac{1}{2},j} + \left(\rho\frac{V}{J}\right)_{i,j+\frac{1}{2}} = 0 \qquad (16)$$

The approximation of the vortex sheet equations is similar.

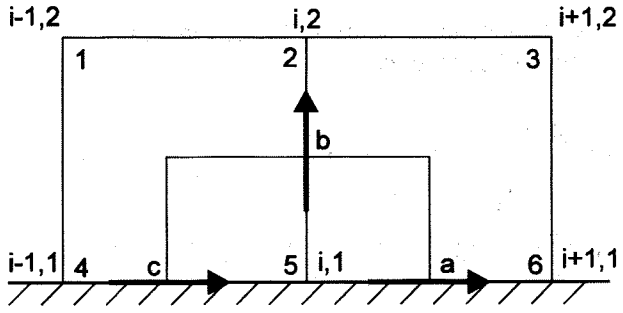

fig.6

Since the numerical procedure of the flow calculation around the wing with flap has special features and requires a presence of two coincident coordinate lines (fig.7), the finite-difference approximation of the equations on these lines differs from the common case.

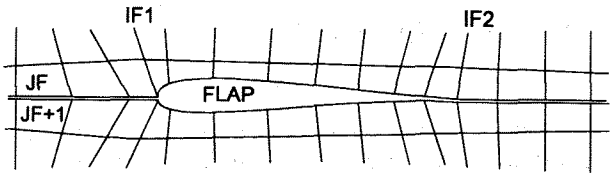

fig.7

Difference equations for the points (i,JF),i=1,..,IF-1 are derived from the mass fluxes balance

$$\bar{\partial}_\xi\left(\frac{\tilde{\rho}U}{J}\right)_{i+\frac{1}{2},JF}+\left(\frac{\rho V}{J}\right)_{i,JF+\frac{3}{2}}-\left(\frac{\rho V}{J}\right)_{i,JF-\frac{1}{2}}=0 \qquad (17)$$

and equations for the points (i,JF+1),i=1,..,IF-1 are derived from the equality of potential on the coincident coordinate lines

$$\varphi_{i,JF+1}=\varphi_{i,JF} \qquad (18)$$

Solution of the equations system

The present non-linear system of finite-difference equations is solved by the iterational method. The linear system, constructed from the non-linear one by means of linearization procedure, is solved at every iteration. In terms of corrections to the potential the linear system has the form

$$AC^n=r^n$$

$$\varphi^{n+1}=\varphi^n+C^n$$

$$r^n=-A\varphi^n \qquad (19)$$

The corrections to the mass fluxes may be expressed as follows

$$\Delta\left(\frac{\tilde{\rho}U}{J}\right)_{i+\frac{1}{2},j}=A^{(--)}_{i+\frac{1}{2},j}\bar{\partial}_\xi C_{i-2}+A^{(-)}_{i+\frac{1}{2},j}\bar{\partial}_\xi C_{i-1}+$$
$$+A^{(0)}_{i+\frac{1}{2},j}\bar{\partial}_\xi C_i+A^{(+)}_{i+\frac{1}{2},j}\bar{\partial}_\xi C_{i+1}+A^{(++)}_{i+\frac{1}{2},j}\bar{\partial}_\xi C_{i+2}$$

$$\Delta\left(\frac{\rho V}{J}\right)_{i,j+\frac{1}{2}}=B^{(0)}_{i+\frac{1}{2},j}\bar{\partial}_\xi C_i$$

Coefficients $A^{(\,)}_{i+\frac{1}{2},j}$ are obtained by means of linearization procedure applied to the mass balance equation. Expressions for corrections to the other fluxes have similar form. Finally, the linear equation for the point (i,j) looks like

$$D^{(1)}_{i,j}C_{i,j}+D^{(2)}_{i,j}C_{i-1,j}+D^{(3)}_{i,j}C_{i+1,j}+$$
$$+D^{(4)}_{i,j}C_{i,j+1}+D^{(5)}_{i,j}C_{i,j-1}+ \qquad (20)$$
$$+D^{(7)}_{i,j}\bar{\partial}C_{i,j}+D^{(8)}_{i,j}\bar{\partial}C_{i,j}=r_{i,j}$$

The terms including $A^{(++)}$, $A^{(--)}$ were not taken into consideration because of their negligible effect on convergence rate. The equation (20) is constructed on 7-points stencil (fig.8). The linear system is solved with the help of incomplete LU-factorization method as it is described by Karas [3]. According to this approach, matrix $\hat{A}$, which is similar to matrix A without taking into account coefficients $D^{(7)}_{i,j}$ and $D^{(8)}_{i,j}$, is approximately presented as a product of lower and upper triangle matrixes L and U. Let $C^{(0)}_{i,j}$ be the initial approximation of the vector of corrections. The next approximation $C^{(1)}_{i,j}$ may be found in the form $C^{(0)}_{i,j}+\delta_{i,j}$, where $\delta_{i,j}$ is determined as follows

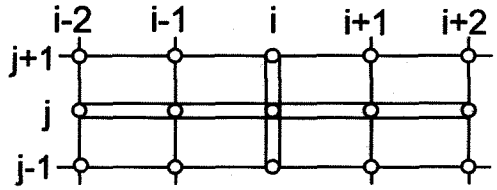

fig.8

(1) forward sweep (fig.9)

$$L^{(1)}_{i,j}s_{i,j}+L^{(2)}_{i,j}s_{i-1,j}+L^{(3)}_{i,j}s_{i,j+1}+$$
$$+L^{(4)}_{i,j}s_{i+1,j+1}=p_{i,j} \qquad (21)$$

where $p=r-AC^{(0)}$, s - temporary variable

(2) backward sweep

$$t_{i,j}+U^{(1)}_{i,j}t_{i+1,j}+U^{(2)}_{i,j}t_{i,j-1}+$$
$$+U^{(3)}_{i,j}t_{i-1,j-1}=s_{i,j} \qquad (22)$$

(3) residual minimization

$$\delta_{i,j} = \text{const}\ t_{i,j} = \frac{(p, \hat{A}t)}{(\hat{A}t, \hat{A}t)} t_{i,j} \qquad (23)$$

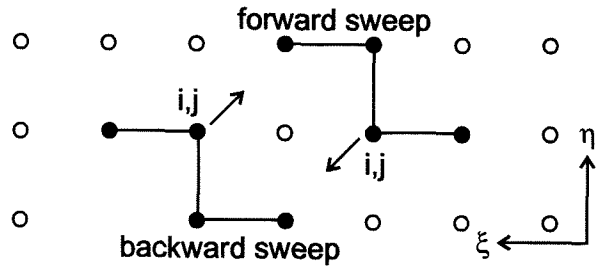

fig.9

$U^{()}_{i,j}$ and $L^{()}_{i,j}$ are coefficients of the triangle matrixes L and U.

We have to assume $s_{i,NY} = s_{0,j} = s_{NX,j} = 0$ to begin the forward sweep. In order to fulfil the backward sweep, it is necessary to determine the values $t_{i,j}$ on the wing surface and on the vortex sheet. For the node (i,1) on the wing surface and the adjacent node (i,2) we define the system of two equations according to (16) and (22). Similarly, for the node (i,1) on the vortex sheet, the adjacent node (i,2) and the according node on the contrary surface of the sheet, the system of three equations is defined. Let's introduce the trailing edge correction difference $\Delta t_{TE} = t_{ITE2,1} - t_{ITE1,1}$ (ITE1 and ITE2 are numbers of trailing edge nodes), which is preserved along the vortex sheet. If $t_{k,1}$, where (k,1) are lower vortex sheet nodes, may be excluded with the use of Δt_{TE}, we may consider the systems for the nodes on the surface and on the vortex sheet as a block-tridiagonal system (3 x 3 blocks) for the unknown three-components vectors

$$\Delta_i = \begin{pmatrix} t_{i,2} \\ t_{i,1} \\ t_{k,2} \end{pmatrix}, i = 1, \ldots, ITE2$$

The right hand part of the system contains unknown value Δt_{TE}. The solution of the system

$$B\Delta = \vec{a} + p_1\vec{b} + p_2\vec{c} + p_3\vec{d}$$

where $p_1 = \Delta t_{TE}$, $p_2 = t_{ITE-1,1}$, $p_3 = t_{ITE2+1,2}$, $\vec{a}, \vec{b}, \vec{c}, \vec{d}$ are known vectors, may be found as a linear combination of particular solutions obtained when the right hand parts equals to vectors $\vec{a}, \vec{b}, \vec{c}, \vec{d}$.

After three steps of the iteration had been accomplished and the vector $\vec{\delta}$ was found, the process of the linear system solution may be completed or continued, depending on the residual value. This approach allows to reduce the residual on 2-3 orders after several iterations.

Figure 10 demonstrates the convergence history of the described method for the non-linear system solution compared with the SLOR and SLOR+GMRES [4] , when applied to the wing without flap. Figure 10 shows the difference of convergence rates of the described method for the wing with and without flap.

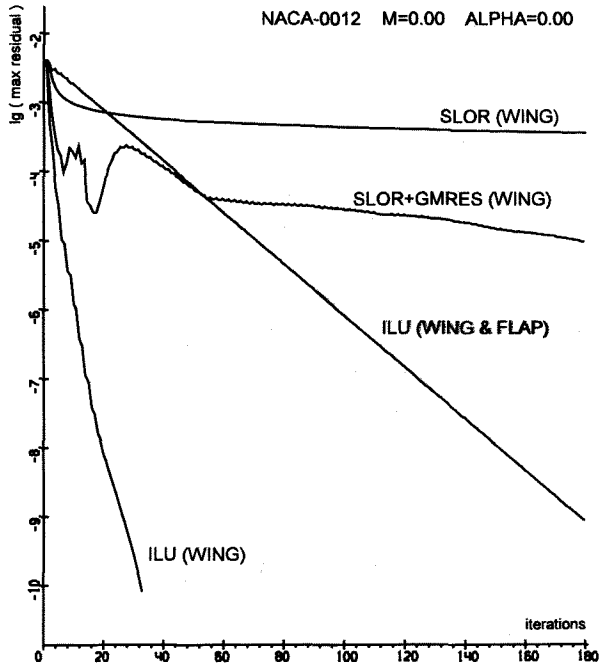

fig.10

Flow analysis examples

Some test examples were accomplished by the current method in order to demonstrate its capabilities. The first test example (fig.11) shows the pressure distribution on the Zhukovsky foil with relative $\overline{C}_{MAX} = 15\%$ at M=0, obtained by the current method, compared with an exact solution. The second example (fig.12) demonstrates the difference between the solution for the transonic regime, calculated by the current method with first and second orders of accuracy in supersonic regions, and the solution, calculated by the Euler solver. It is evident, that not very intensive shocks are approximated much more qualitative, when the numerical scheme of the 2nd order of accuracy is

applied. The last test example (fig.13) demonstrates calculation of the flow around an infinite wing with flap compared with the results obtained by the panel solver.

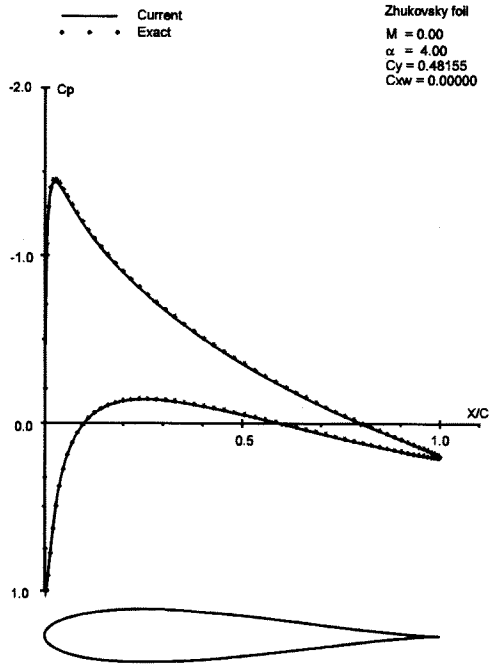

fig.11

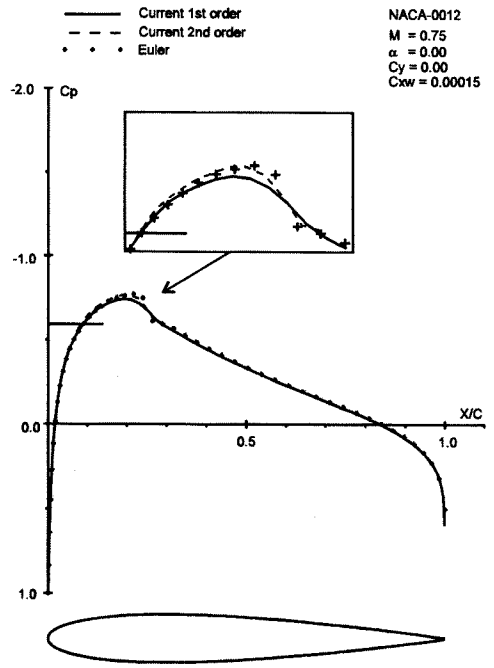

fig.12

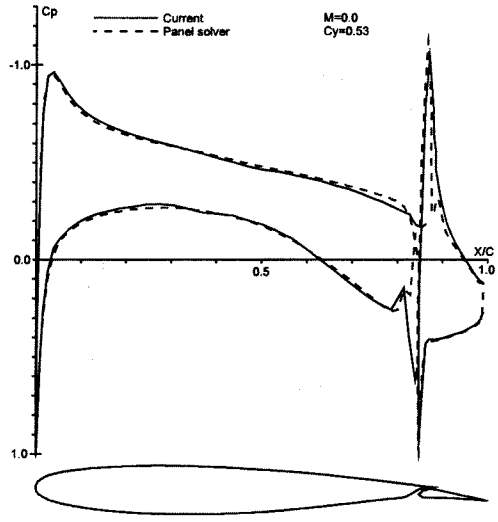

fig.13

Inverse problem

Specification of combined boundary conditions

In order to solve the design problem by the described method it is necessary to specify combined boundary conditions on the surface, according to which the specified pressure distribution is fixed on the part of the surface, fixed by designer. Obtaining from the expression for Cp speed sqared

$$q^2 = 1 - \frac{2}{(\gamma-1)M_\infty^2}\left[\left(1+\frac{\gamma M_\infty^2 C_P}{2}\right)^{\frac{\gamma-1}{\gamma}} - 1\right] \quad (24)$$

and taking into account that

$$q^2 = U\varphi_\xi + V\varphi_\eta$$
$$U = A_1\varphi_\xi + A_2\varphi_\eta$$
$$V = A_2\varphi_\xi + A_3\varphi_\eta$$

we find the derivative of the potential along the surface as a boundary condition on the designed part of the surface

$$\varphi_\xi\big|_W = \pm\left[\frac{A_3 q^2 - \tilde{V}^2}{A_1 A_3 - A_2^2}\right]^{1/2} \quad (25)$$

where $\tilde{V}$ is the normal velocity, determined in the iterational process. The sign of the derivative is defined depending on the direction of the velocity in the corresponding point of the surface.

Normal velocity surface distribution

When solving the system of the equations of potential with the combined boundary conditions, the no flux condition is not valid on the designed part of the surface, and the distribution of the normal contravariant velocity component $\tilde{V}$ may be found at every iteration from the expression

$$\tilde{V}_{i+\frac{1}{2},1} = \frac{J_{i+\frac{1}{2},1}\left(r_{i,1} + r_{i+1,1}\right)}{2\tilde{\rho}_{i+\frac{1}{2},1}} \qquad (26)$$

where $r_{i,1}$ are residuals, calculated in the points of the surface.

Wing shape correction

After the system with combined boundary conditions has been solved, it is necessary to correct the wing shape taking into account the calculated values of normal velocities. The new local angle of the slope of the surface must be equal to the angle between the Ox axis and velocity vector in the current point (fig.14).

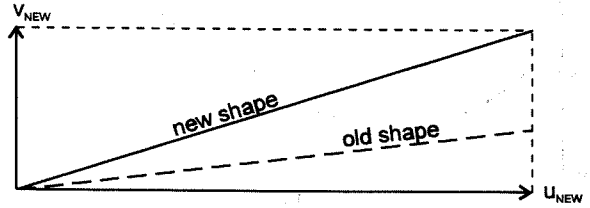

fig.14

Consiquently, the equation (27) must be valid.

$$\Delta\left(\frac{dy}{dx}\right)_i = \left(\frac{dy}{dx}\right)_i^{NEW} - \left(\frac{dy}{dx}\right)_i^{OLD} = \left(\frac{v}{u}\right)_i \qquad (27)$$

The analogue of this expression in the curvilinear coordinate system looks like

$$\Delta\left(\frac{dy}{dx}\right)_i = \left\{\frac{J\left(\frac{V}{U}\right)}{x_\xi\left(x_\xi + x_\eta\left(\frac{V}{U}\right)\right)}\right\}_i \qquad (28)$$

The result of integration of the expression (28) along the designed part of the wing surface is the new shape of this part of the wing.

Trailing edge closure

Since not every pressure distribution corresponds to the foil with the closed trailing edge, it is possible to obtain the foil with too thick or, on the contrary, crossed itself trailing edge as a result of the design procedure. In such case it is necessary to apply the trailing edge closure procedure, which slightly changes the pressure distribution. But using any geometrical transformation for this purpose, for example, as described by Gally and Carlson [5],

$$y^{CLOS} = y^{NEW} - (y_{TE}^{NEW} - y_{TE}^{OLD})\frac{x}{c} \qquad (29)$$

where C - chord (fig.15), results in a low convergence rate of the design procedure.

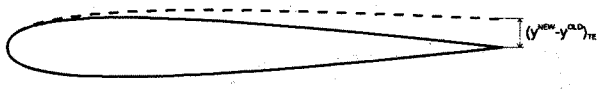

fig.15

In the present paper another method is applied, offered by Karas [3], according to which the value of the trailing edge deviation, corresponding to the current normal velocity distribution, is determined at every iteration of the solution of the system with the combined boundary conditions, and then the normal velocity distribution is modified, so that the corresponding trailing edge deviation is equal to zero. This modification is fulfilled with the help of the additional function of the normal velocity distribution, which slightly changes the pressure distribution, for example, corresponding to the transformation (29).

Design regimes

This approach allows us to use the normal velocity distribution corrections both for the trailing edge closure procedure and for taking into account some other geometrical restrictions. In particular, using this methodology we can maintain thickness or camber distributions chordwise, when designing only one of two surfaces. Also by automatical adding a small function $\Delta C_P^{(Cy)}$ to the specified C_P distribution we can easily maintain the specified Cy during the design process. In order to use largely all these advances of the current approach, this method has three design regimes:

(a) One surface (or its part) design maintaining thickness distribution and Cy;

(b) One surface (or its part) design maintaining camber distribution and Cy;

(c) Both surfaces (or their parts) design without geometrical restrictions maintaining Cy.

To maintain Cy is not a necessary condition, but has large practical value. All these features make this

design method flexible enough for an effective use on the preliminary design step.

Design examples and discussion

A series of test design examples were accomplished in order to demonstrate abilities of the design method described.
First two examples (fig.16,17) demonstrate the ability of design of one-element airfoils. The geometry of the airfoil RAE-2822 was taken as an initial geometry.
In the first design case (fig.16) a subcritical airfoil was designed.

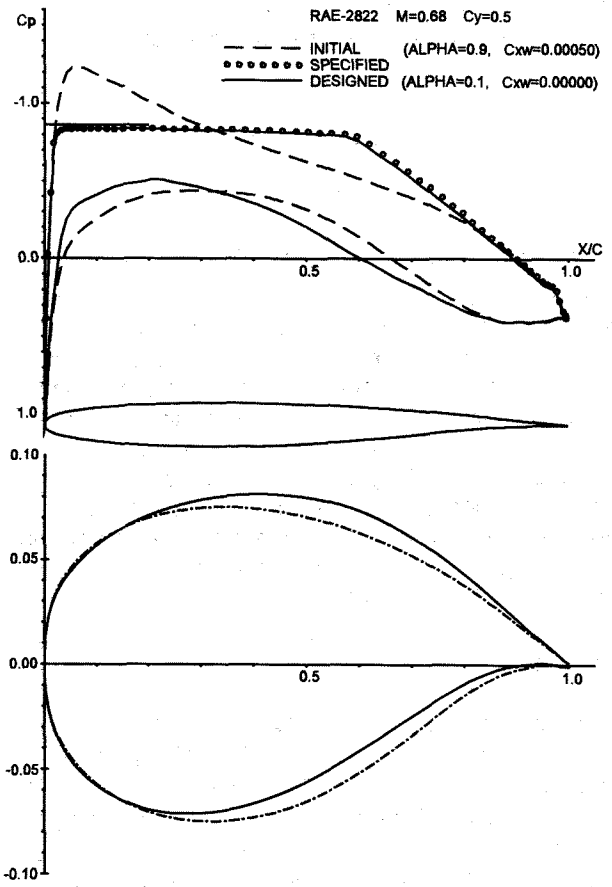

fig.16

The analysis of the flow around the initial airfoil was carried out under conditions M_∞ =0.68, Cy=0.5. At this regime a supersonic region on the upper surface of the foil appeared. The target pressure distribution was fixed only on the upper surface and was selected from the conditions of supersonic regions absence and pressure gradient near the trailing edge restriction

$$\frac{dC_P}{dx} \le 2.3^{(6)} \qquad (30)$$

in order to avoid a boundary layer separation. The lower surface was used to maintain thickness distribution. This design case shows the ability of the current method to design a subsonic airfoil from a transonic one.

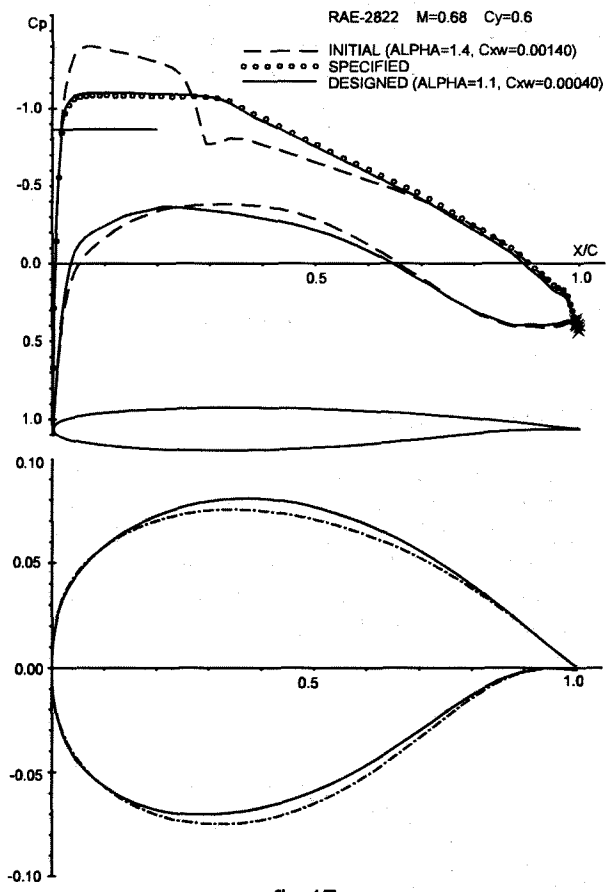

fig.17

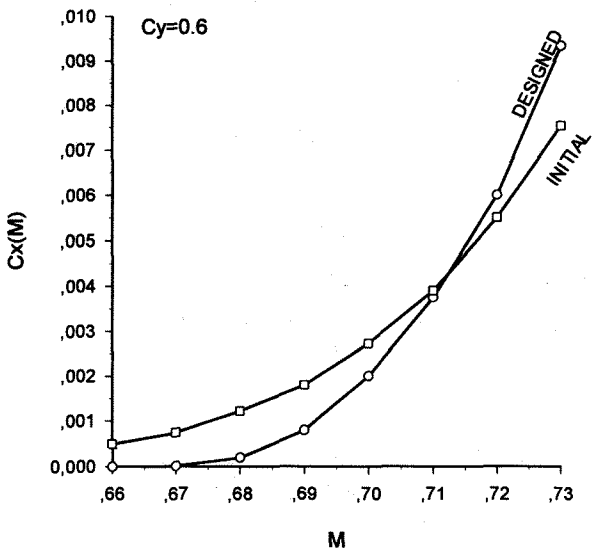

fig.18

The second design case (fig.17) demonstrates the ability of supercritical design.
The analysis of the flow around the initial airfoil was carried out under conditions M_∞ =0.68, Cy=0.6. Now not very strong shock appeared on the upper surface, and the target pressure distribution was also fixed only on the upper surface and was selected from the conditions of pressure gradient near the trailing edge restriction (30) and shocks absence. The lower surface was used to maintain thickness distribution. At this regime a supersonic region takes place on the upper surface, but the value of wave drag is essentially smaller. This fact is confirmed by the plot of the designed airfoil wave drag as a function of Mach number (fig.18), compared with the same dependence for the initial airfoil.

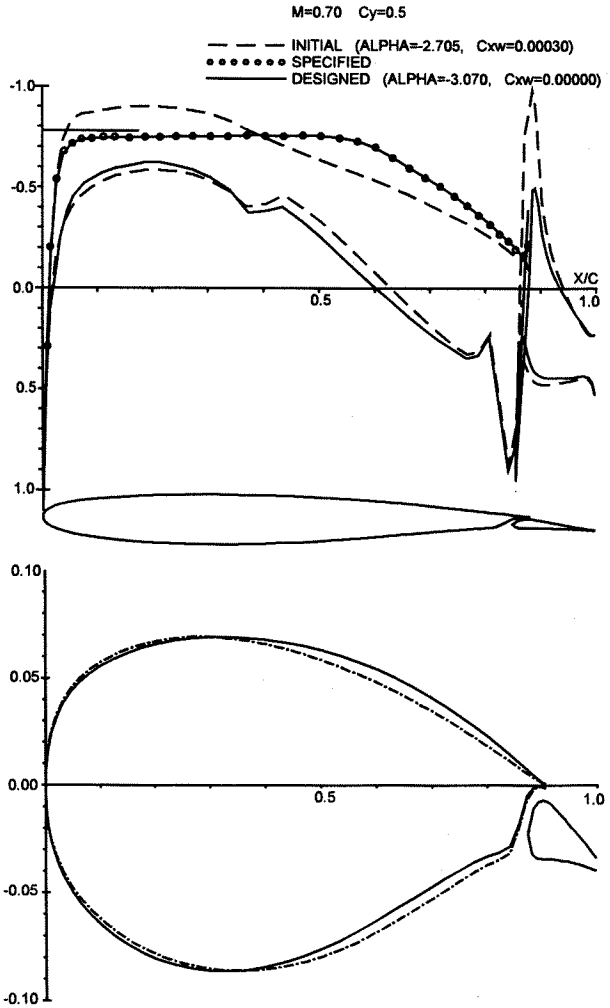

fig.19

Unfortunately, large pressure value on the trailing edge does not allow us to enlarge a pressure plateau on the upper surface and, consequently, to design airfoils at harder conditions because of the pressure gradient restriction. Diminishing pressure on the trailing edge of the upper surface at the boundary layer separation absence would allow us to fix the target pressure distribution with longer pressure plateau and shorter pressure gradient part. As fig.13 shows, this problem may be partly solved by means of a flap usage. The next design cases demonstrate the ability of the design of airfoils with flap for cruise flight regimes. A foil with flap, obtained from the airfoil RAE-2822, was used as an initial configuration. The relative chord lenght of the main element was equal 0.88, of the flap - 0.15.

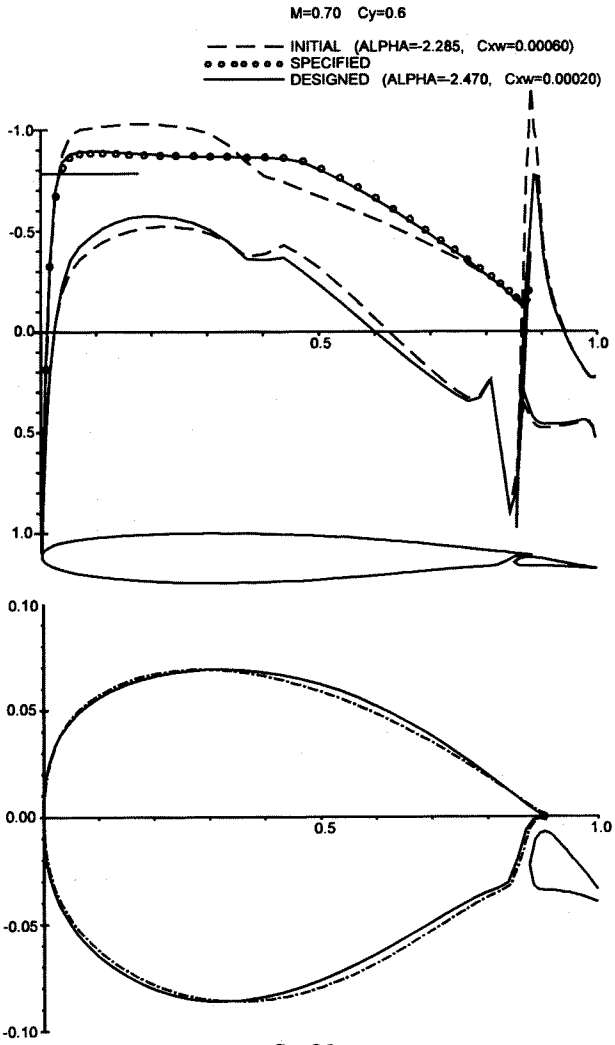

fig.20

In the third design case (fig.19) the ability of subsonic airfoil with flap design was demonstrated. The analysis of the flow around the initial configuration was carried out under conditions M_∞ =0.70, Cy=0.5. Lower surface was used to maintain thickness distribution, and on the upper surface the target pressure distribution was fixed, which was selected from the condition of subsonic flow, and the pressure gradient near the trailing edge of the main element was much smaller than in preceding cases. This design case has the same features as the first one, but a presence of flap

allowed us to accomplish design at larger Mach number.
The fourth design case (fig.20) demonstrates the ability of transonic design without shocks for the airfoil with flap. The flow analysis conditions were M_∞ =0.70, Cy=0.6. The lower surface was used to maintain thickness distribution, and on the upper surface the target pressure distribution was fixed, which was selected from the condition of shock absence, and pressure gradient near the trailing edge of the main element, like in preceding case, was small. A presence of a flap also allowed us to design at larger Mach number.

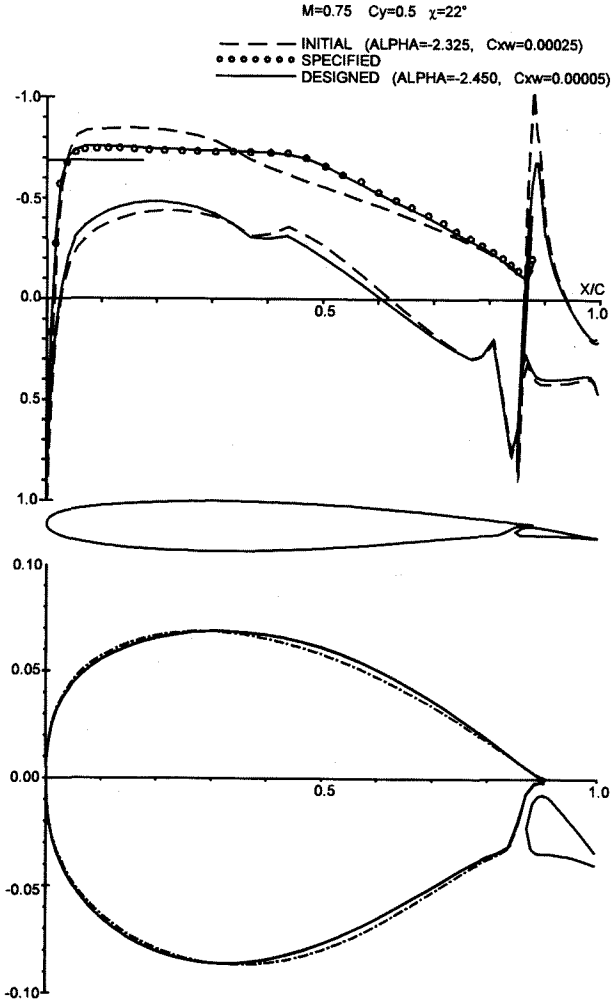

fig.21

The fifth design case (fig.21) demonstrates the ability of the design swept infinite wing. The flow analysis conditions were M_∞ =0.75, Cy=0.6, χ=22°. The design conditions are the same as for the fourth design case.
The test design examples show that transonic design with flap at the same design conditions may give an advantage, for example, in Mach numbers, and an important conclusion may be done: in a course approximation it is possible to use flap for cruise regimes, and investigations in this direction may be continued.

Summary

In spite of a series of useful features of the current method, one of its most remarkable disadvantages is an absense of taking into consideration of a viscous effects. That is why a subject of the nearest future work on improval of this method will be including viscous effects by means of using viscous-inviscid interaction procedure. This will enlarge a practical value of the method described.

Acknowledgements

The author greatly appriciates the many helpful recommendations and comments of Dr. V. E. Kovalev, Dr. O. V. Karas and Dr. S. V. Lyapunov, Central Aerohydrodynamics Institute (TsAGI), Russia.

References

1. Jameson A., Caughey D. A., Numerical Calculation of the Transonic Flow Past a Swept Wing, New York University ERDA report COO-3077-140, June 1977.
2. Osher S., Hafez M., Whitlow W. Enthropy Condition Satisfying Approximations for the Full Potential Equation of Transonic Flow, Mathem. of Computation, 1985. v. 44, N 169, p. 1-29.
3. Karas O. V., Central Aerohydrodynamics Institute, private communications.
4. Y. Saad, M. H. Schultz, GMRES: A generalized Minimal Residual Algorithm for Solving Nonsymmetric Linear System, Research Report YALEU/DCS/RR-254, August 24, 1983.
5. Gally T. A., Carlson L. A., Inviscid Transonic Wing Design Using Inverse Methods in Curvilinear Coordinates, Paper 87-2551, AIAA 5th Applied Aerodynamics Conference, Monterey, CA, Aug. 17-19, 1987.
6. S. Obayashi, S. Takanashi, Genetic Optimization Of Target Pressure Distributions For Inverse Design Methods, AIAA-95-1649-CP, 1995.